



저작자표시-비영리-동일조건변경허락 2.0 대한민국

이용자는 아래의 조건을 따르는 경우에 한하여 자유롭게

- 이 저작물을 복제, 배포, 전송, 전시, 공연 및 방송할 수 있습니다.
- 이차적 저작물을 작성할 수 있습니다.

다음과 같은 조건을 따라야 합니다:



저작자표시. 귀하는 원저작자를 표시하여야 합니다.



비영리. 귀하는 이 저작물을 영리 목적으로 이용할 수 없습니다.



동일조건변경허락. 귀하가 이 저작물을 개작, 변형 또는 가공했을 경우에는, 이 저작물과 동일한 이용허락조건하에서만 배포할 수 있습니다.

- 귀하는, 이 저작물의 재이용이나 배포의 경우, 이 저작물에 적용된 이용허락조건을 명확하게 나타내어야 합니다.
- 저작권자로부터 별도의 허가를 받으면 이러한 조건들은 적용되지 않습니다.

저작권법에 따른 이용자의 권리는 위의 내용에 의하여 영향을 받지 않습니다.

이것은 [이용허락규약\(Legal Code\)](#)을 이해하기 쉽게 요약한 것입니다.

[Disclaimer](#)

Thesis for the Degree

Master of Education

**Investigation of NH_4OH on Zircaloy-4
Surface using Electron
Spectroscopies**



by

Hye Yoon Jung

Graduate School of Education

Pukyong National University

August 2007

**Investigation of NH_4OH on Zircaloy-4 Surface
using Electron Spectroscopies**

**전자 분광학을 이용한 수산화암모늄과
지르칼로이-4의 표면 분석**

Advisor : Prof. Yong-Cheol Kang

by

Hye Yoon Jung

A thesis submitted in partial fulfillment of the requirements
for the degree of

Master of Education

Graduate School of Education
Pukyong National University

August 2007

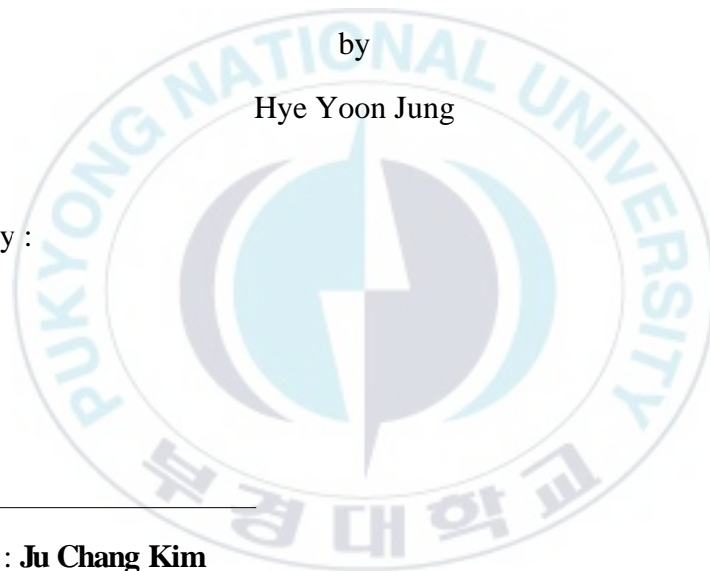
**Investigation of NH₄OH on Zircaloy-4 Surface
using Electron Spectroscopy**

A dissertation

by

Hye Yoon Jung

Approved by :



(Chairman) : **Ju Chang Kim**

(Member) : **Don Kim**

(Member) : **Yong-Cheol Kang**

August 30, 2007

Contents

List of Figures.....	iii
List of Table	vi
abstract	vii
I . Introduction	1
II . Theory	3
2.1 Auger Electron Spectroscopy	3
2.1.1 The Auger process	3
2.1.2 Auger electron energies	5
2.1.3 Auger surface sensitivity	6
2.2 X-ray Photoelectron Spectroscopy	7
III. Experimental	11
3.1 Auger electron spectroscopy of Zircaloy-4	11
3.1.1 Experimental apparatus	11
3.1.2 Experimental procedure	14
3.2 Investigation of NH₄OH on Zircaloy-4 Surfaces using	
X-ray Photoelectron Spectroscopy	15
3.2.1 Preperation of sample and operation of XPS	15
3.2.2 Deconvolution	16

IV. Results and Discussion	17
4.1 Auger electron spectroscopy of Zircaloy-4	17
4.2 Investigation of NH ₄ OH on Zircaloy-4 Surfaces using X-ray Photoelectron Spectroscopy	22
V. Conclusion	35
VI. Reference	36
VII. Appendices	38
Appendix A : Procedure for Argon ion sputtering	38
Appendix B : Procedure for Auger electron spectroscopy (AES) experiments	40
Appendix C : Eurotherm PID setting	42
Appendix D : TPD experiment	43
Korean Abstract	44
Acknowledgement	45

List of Figures

Figure 2.1	Energetic of the Auger process.	4
Figure 2.2	Auger and x-ray fluorescence yields as a function of atomic number. The solid lines show Auger yields; the dashed lines, fluorescence yield.	5
Figure 2.3	The interaction between an incident electron beam and a solid sample, showing the analysis volumes for Auger electrons, secondary electrons, backscattered electrons, and x-ray fluorescence.	7
Figure 2.4	X-ray excitation of a 1s core level.	9
Figure 2.5	Electrostatic energy analyser used in electron/ion spectroscopic analysis of surfaces.	10
Figure 3.1	Schematic representation (front view) of the ultra-high system for LEED/AES.	12
Figure 3.2	Schematic representation (top view) of the ultra-high system for LEED/AES.	13
Figure 4.1	The survey AE spectra of Zry-4 before and after stepwise argon ion sputtering. The numbers at the right in the figure present Ar fluence.	18

Figure 4.2	APPH ratios of Zircaloy-4 surfaces function of Ar ⁺ fluence (a) O(KLL)/Zr(MNV), (b) C(KLL)/Zr(MNV) and (C) N(KLL)/Zr(MNV).	19
Figure 4.3	The survey XP spectra of NH ₄ OH/Zry-4 before and after Ar ⁺ sputtering with LAXPS mode. The numbers at the left in the figure represent Ar fluence.	21
Figure 4.4.1	(a) stacked XP spectra of the N1s region after argon ion sputtering processes indicate a strong increase of N1s.	23
Figure 4.4.2	Deconvoluted XP spectra of the N1s region in NH ₄ OH/Zry-4 (b) after 0.8 x 10 ¹⁶ Ar ⁺ sputtering and (c) after 9.75 x 10 ¹⁶ Ar ⁺ sputtering. Wiggly lines in (b) and (c) represent raw data, smooth lines overlapped with raw data are reconstructed data and bottom solid lines are background. N1s of ammonia is centered at 387.1 eV and N 1s of nitride is centered at 398.9 eV. participating in hydrogen bonding are omitted for clarity.	24
Figure 4.5.1	(a) XP spectra of the O1s region after argon ion sputtering indicates a strong reduction of O1s.	26
Figure 4.5.2	Deconvoluted XP spectra of the O1s region in NH ₄ OH/Zry-4 (b) before and (c) after Ar ⁺ sputtering.	27

Wiggly lines in (b) and (c) represent raw data, smooth lines overlapped with raw data are reconstructed data and bottom solid lines are background. The component centered at 531.0 eV is attributed to the hydroxyl ion and 532.8 eV is attributed to the presence of O^{2-} ions.

Figure 4.6.1 (a) XP spectra of the Zr3d region following cycles of Ar⁺ sputtering. XPS spectra of the Zr3d region in NH₄OH/Zry-4 (b) before and (c) after Ar⁺ sputtering. 29

Figure 4.6.2 Wiggly lines in (b) and (c) represent raw data, smooth lines overlapped with raw data are reconstructed data and bottom solid lines are background. Zr3d of metallic zirconium is centered at 179.1 eV, Zr3d of ZrN_x is centered at 181.6 eV, Zr3d of ZrO_x is centered at 398.9 eV and Zr3d of Zr⁴⁺ zirconia is centered at 183.4 eV. 30

Figure 4.7 The area of deconvoluted XPS peaks of NH₄OH/Zry-4 surface as a function of argon fluence (a) N1s, (b) O1s and (c) Zr3d. 34

List of Table

Table 1	Comparison of physical properties of Group IV metals, iron and tantalum.	1
----------------	--	---



Investigation of NH₄OH on Zircaloy-4 Surface using Photoelectron Spectroscopy

Hye Yoon Jung

Graduate School of Education

Pukyong National University

Abstract

The interaction of Ammonium hydroxide (NH₄OH) with Zircaloy-4 (Zry-4) was investigated using X-ray Photoelectron Spectroscopy (XPS) and the surface cleanness was checked by Auger Electron Spectroscopy(AES). In order to study surface chemistry of NH₄OH/Zry-4 system, the binding energies of N 1s, O 1s and Zr 3d electrons were monitored. The N 1s peak intensity remarkably increased following cycles of argon ion sputtering after NH₄OH dosed onto Zry-4 surface at room temperature because the nitrogen stayed under the surface region was diffused out onto the Zry-4 surface. But, the surface oxygen was diffused into the bulk or desorbed out until Ar⁺ fluence was 6.0×10^{16} Ar⁺/cm². Therefore the O 1s peak intensity was decreased by stepwise Ar⁺ sputtering. After many cycles of Ar⁺ sputtering, the peak intensities of Zr 3d peaks were not changed but the shapes of the peaks were clearly changed. This implies that the oxidation state of zirconium is changed during Ar⁺ sputtering. The Zr 3d peak intensity of zirconium nitride (ZrN_x) increased as the intensity of N 1s (from zirconium nitride) increased but the Zr 3d peak intensity of zirconium oxide (ZrO_x) decreased due to depopulation of the hydroxyl ion. The Zr⁴⁺ intensity was nearly same after Ar⁺ sputtering processes but the peak intensity of metallic Zirconium increased compared to that of before the sputtering process because the surface was relatively clean.

I . Introduction

The alloys of zirconium have been developed for use as cladding material and structural material in nuclear reactors because of their low thermal neutron cross section and the corrosion resistance [1-8].

	²² Ti	⁴⁰ Zr	⁷² Hf	²⁶ Fe	⁷³ Ta
Melting point (K)	1933	2128	2500	1808	3270
Boiling point (K)	3560	4682	4875	3023	5698
Thermal conductivity (W/m K)	21.9	23.0	23.0	80.0	57.5
Linear expansion coefficient (K-1)	8.9×10^{-6}	5.7×10^{-6}	6.0×10^{-6}	1.2×10^{-7}	6.5×10^{-6}
Thermal neutron cross-section (bars) [1 barn = 1×10^{-24} cm ²]	6.1	0.2	106.3	2.6	22

Table 1 Comparison of physical properties of Group IV metals, iron and tantalum [9].

Zr-alloys are also known to dissolve large amounts of oxygen and hydrogen [10-15] and the interactions of these species on the surface and zircaloy surfaces are considered to control the environmental degradation of the alloys [16-18]. According to the fact that these alloys usually cause embrittlement of the structural components.

The reprocessing of spent nuclear fuel can involve high concentrations of nitrate, ammonium, peroxide ions and other reactive species such as chloride [19] and Zircaloy-4 (Zry-4) is often used to construct the containment vessel for these and many other chemicals in engineering applications [20]. The contact of oxygen, nitrogen and hydrogen containing species with zircaloy is common to these industrial

uses of zirconium, and understanding how these species chemically react on zirconium surface is important for technological progress in the nuclear and chemical engineering communities [21].

Removing impurities from the surface and subsurface regions of zirconium and its alloys has always been a challenge. Cleaning zirconium and its alloys are exceptionally difficult since high-temperature annealing of zirconium-based materials results in the dissolution of surface oxygen, carbon, [27] and nitrogen atoms [21].

Consequently, a number of group studied the behavior of H₂O, D₂O and NH₃ on the alloys of zirconium [21-25]. Despite the fact that many results have been published on the subject, little is known about the surface chemistry of NH₄OH which is using for pH controlling reagent [26] on zirconium-based materials in nuclear industry. However these are relevant issues due to the gettering nature of zirconium for oxygen and nitrogen segregation from the bulk to the near-surface region at high temperature [27]. In addition , much of the work investigating the interaction of ammonia on the latter transition-metal surfaces has concentrated on NH₃ adsorption states; comparatively little is known about the thermal chemistry of ammonia on those surfaces [28].

The argon ion sputtering effect was investigated after 90 Langmuir (1 L = 1.0x10⁻⁶ torr s) of NH₄OH dosed on Zry-4 surface by using XPS and the adsorption of NH₄OH dosed on Zry-4 surface, in particular C, N, O and Zr, at a temperature relevant to nuclear application (893K). AES experiments were conducted under ultra-high vacuum conditions and check the surface cleanness.

II . Theory

2.1 Auger Electron Spectroscopy

2.1.1 The Auger process

In Auger electron spectroscopy (AES), electrons are detected after emission from the sample as the result of non-radiative decay of an excited atom in the surface region. An inter-atomic process in the production of an Auger electron is shown in Figure 2.1. The atom is raised into an excited state by the creation of a core hole, as a result of an interaction with either an incident X-ray photon or high energy electron. An electron then falls in energy from a higher level to fill this core hole, and the excess energy is carried away as the kinetic energy of a further electron which is emitted from the atom. The use of the electron beam as the primary method of excitation in AES gives the technique one of its most powerful attributes, namely high spatial resolution. The beam can be scanned, as in the scanning electron microscope, and, by tuning the analyser to detect Auger electron from the elements of interest, compositional maps of surface concentration can be built up.

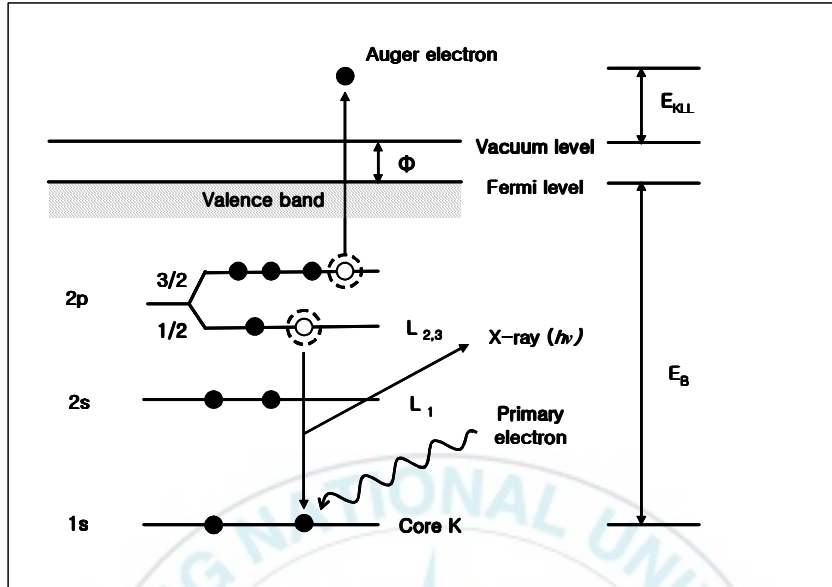


Figure 2.1 Energetic of the Auger process.

Currently, the state of the art limit of resolution is in the range 50-100 nm, although much useful work is carried out with beam diameters around 1 μm . The sum of the total Auger yield and the fluorescence yield is unity, since an excited ion can relax by either Auger electron emission or x-ray emission. Auger electron emission is the more probable decay mechanism for low energy transition, i.e., for low atomic number elements with an initial vacancy in the K shell and for all elements with initial vacancy in the L or M shells. The variation in Auger and x-ray fluorescence yields with atomic number for initial vacancies in the K, L and M shells is shown in Figure 2.2. By choosing an appropriate Auger transition, all elements (except H and He) can be detected with high sensitivity.

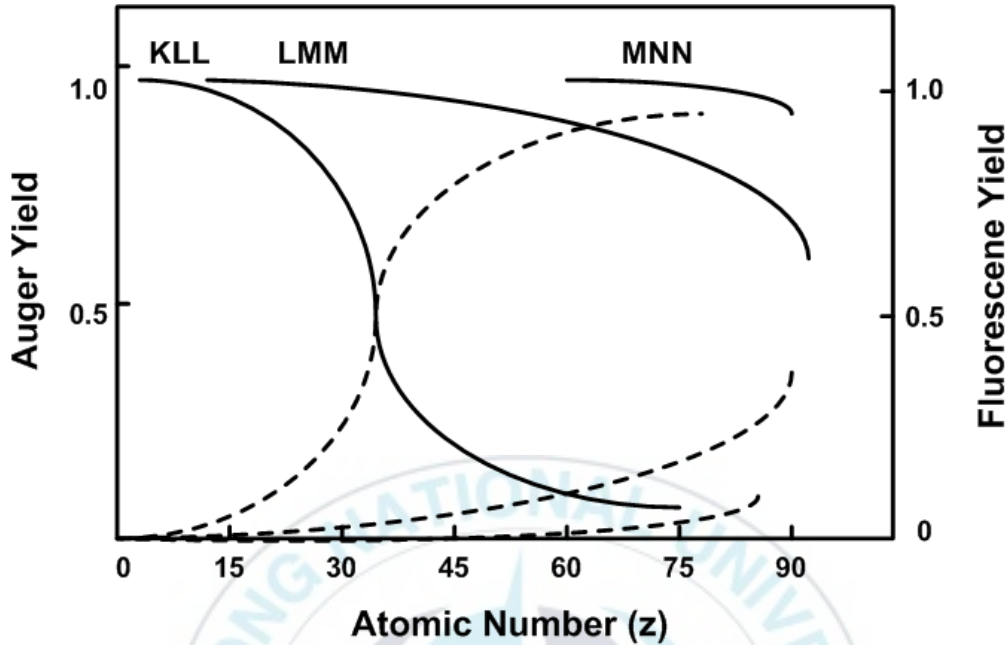


Figure 2.2 Auger and x-ray fluorescence yields as a function of atomic number. The solid lines show Auger yields; the dashed lines, fluorescence yield.

2.1.2 Auger electron energies

The observed energy of an Auger transition is the best approximated with reference to Figure 2.1. Note that the energy scale is referenced to the Fermi level. The primary electron must have sufficient energy to ionize the core level of energy E_K . An electron at energy E_K , fills the initial hole and the energy liberated in this process is transferred to an electron at EL_1 , which is then ejected into the vacuum. This electron must overcome the work function of the sample, Φ , to be released into the vacuum; hence the kinetic energy is reduced by this amount. The vacuum level is constant and electrical contact between

the sample and the analyser leads to alignment of their Fermi levels. Thus it is actually Φ that must be subtracted from the energy of the electron to arrive at the final kinetic energy

$$E_{KLL} = E_K - EL_1 - EL_{12} - \Phi$$

2.2.3 Auger surface sensitivity

Electrons emitted in the solid must be transported to the surface in order to escape the solid and be analyzed. Such electrons may undergo scattering events by interaction with the electrons in the solid. These interactions depend on the energy of the transported electrons and on the matrix electron density. The surface sensitivity of Auger electron spectroscopy arises from the relatively short inelastic mean free path for Auger electrons. The inelastic mean free path is seen to increase with increasing kinetic energy and decrease in matrices of increasing average atomic number.

Figure 2.3 illustrates the interaction of an incident electron beam with a solid sample. The size and shape of this interaction volume is dependent on the primary beam energy and the sample material. The teardrop shape shown here is typical for high primary electron energies incident on low atomic number material. As the atomic number increase or the electron energy decreases, the interaction volume is reduced and appears more like a sphere subtended by the surface. Figure 2.3 shows the regions from which characteristic Auger electrons, secondary electrons, backscattered electrons, and x-ray photons emerge [29].

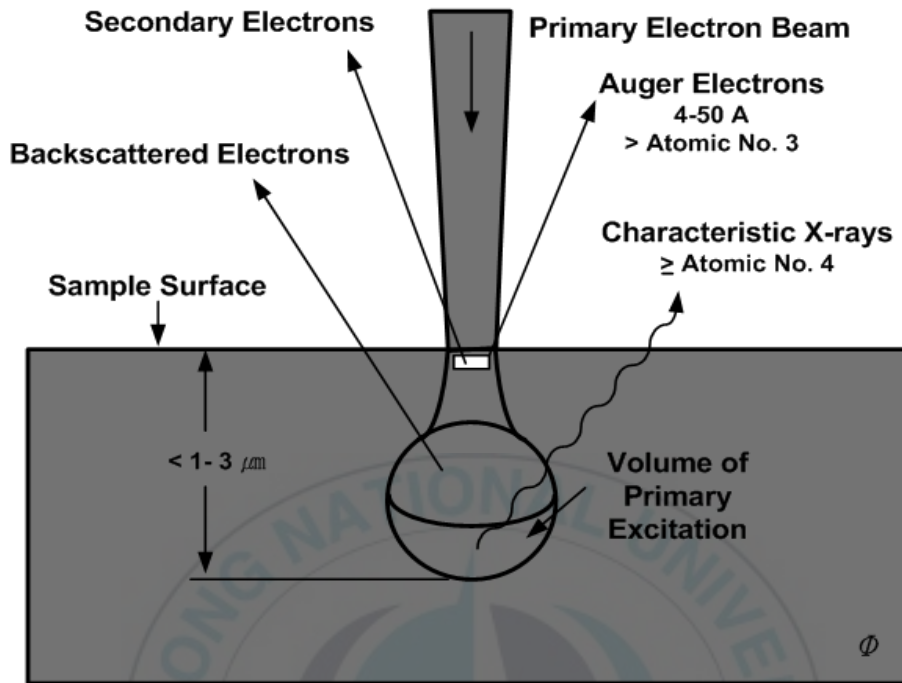


Figure 2.3 The interaction between an incident electron beam and a solid sample, showing the analysis volumes for Auger electrons, secondary electrons, backscattered electrons, and x-ray fluorescence.

2.2 X-ray Photoelectron Spectroscopy

X-ray Photoelectron Spectroscopy (XPS) is one of electron spectroscopies, in which an excitation leads to the ejection of an electron from the solid. The basis of the technique lies in Einstein's explanation of the photoelectric effect, where by photons can induce electron emission from a solid provided an X-ray photon of energy ($h\nu$). The energy of the emitted photoelectrons is then analysed by the electron spectrometer and the data presented as a graph of intensity versus electron energy - the X-ray induced photoelectron spectrum.

Applying the principle of energy conservation (Einstein's photoelectric equation), one may estimate the kinetic energy of emitted photoelectrons (E_{KIN}):

$$E_{\text{KIN}} = h\nu - (E_{\text{B}} + \Phi)$$

where $h\nu$ is the photon energy,

E_{B} is the binding energy of electron in solid

Φ is the spectrometer work function.

The kinetic energy (E_{KIN}) of the electron is the experimental quantity measured by the spectrometer, but this is dependent on the photon energy of the X-rays employed and is therefore not an intrinsic material property. The binding energy of the electron (E_{B}) is the parameter which identifies the electron specifically, both in terms of its parent element and atomic energy level. The relationship between the parameters involved in the XPS experiment is :

$$E_{\text{B}} = h\nu - E_{\text{KIN}} - \Phi$$

The process of photoemission is shown schematically in Figure 2.4, where an electron from the core level is ejected from the atom (a 1s core photo electron).

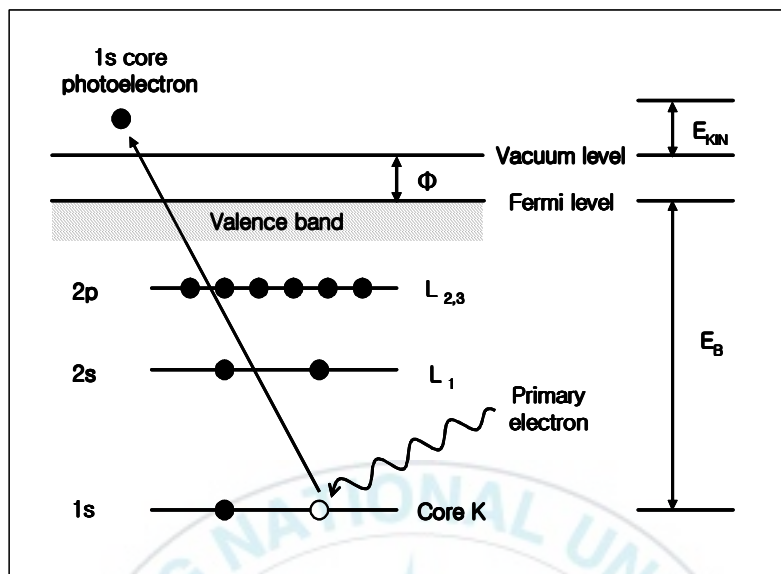


Figure 2.4 X-ray excitation of a 1s core level.

The electron energy distribution [the number of electrons detected 'N(E)' as a function of their kinetic energy] can be measured using an electrostatic energy analyser consisting of two electrically isolated concentric hemispheres with a potential difference between them, as shown in Figure 2.5 The electrostatic field separates electrons by allowing only electrons of a chosen kinetic energy (the 'pass energy') through to the detector (continuous line). While it is the kinetic energy of the outgoing electrons that is measured, spectra are usually displayed on a binding energy scale to allow ease of elemental identification [30].

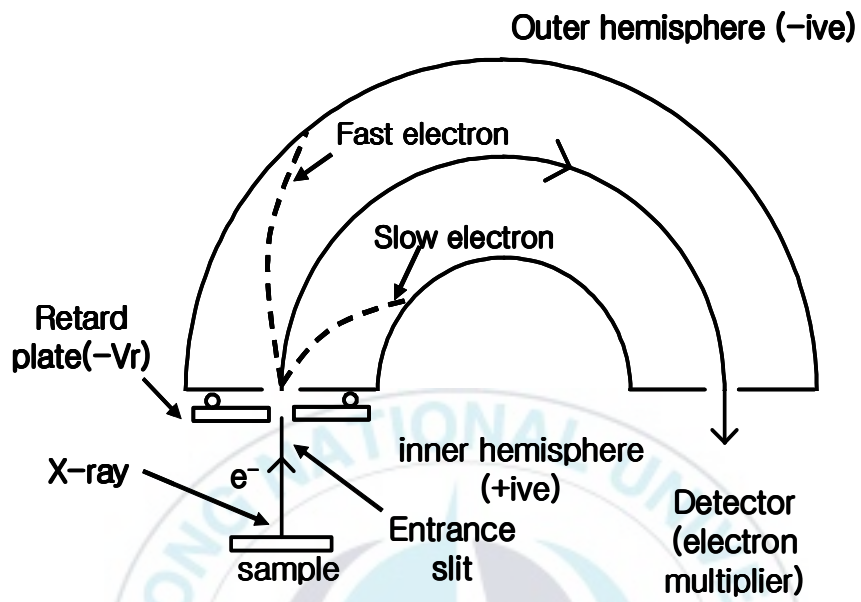


Figure 2.5 Electrostatic energy analyser used in electron/ion spectroscopic analysis of surfaces.

III. Experimental

3.1 Auger electron spectroscopy of NH_4OH on Zircaloy-4

3.1.1 Experimental apparatus

Experiments were conducted in a stainless-steel ultra-high chamber (base pressure $\sim 1.0 \times 10^{-10}$ torr) in this work. The system consist of two separate chambers isolated by gate valve. Most of the analytical tools were housed in the main chamber . These include a combined low energy electron (LEED) and Auger electron spectroscopy (AES) system, a quadruple mass spectrometer (QMS) for temperature programmed desorption (TPD), study an Argon ion sputtering gun for sample cleaning. The vacuum chamber was also equipped with a manipulator that allows limited sample motion along three orthogonal axes and provides rotational capability about the manipulator axis. The base pressure was achieved by two sets of pumps. The first set consist of a water-cooled turbomolecular pump (TMP) backed by a two stage rotary roughing pump (RP). The second set included an ion getter pump and a titanium sublimation pump. Tantalum wires, spot-welded to the sample, were used for dc heating. Two type-K thermocouples, also spot-welded to the sample, were part of a temperature-control feedback loop. Sample cooling was performed by means of a copper braid connected to a liquid-nitrogen cold finger and electrically isolated by sapphire glass.

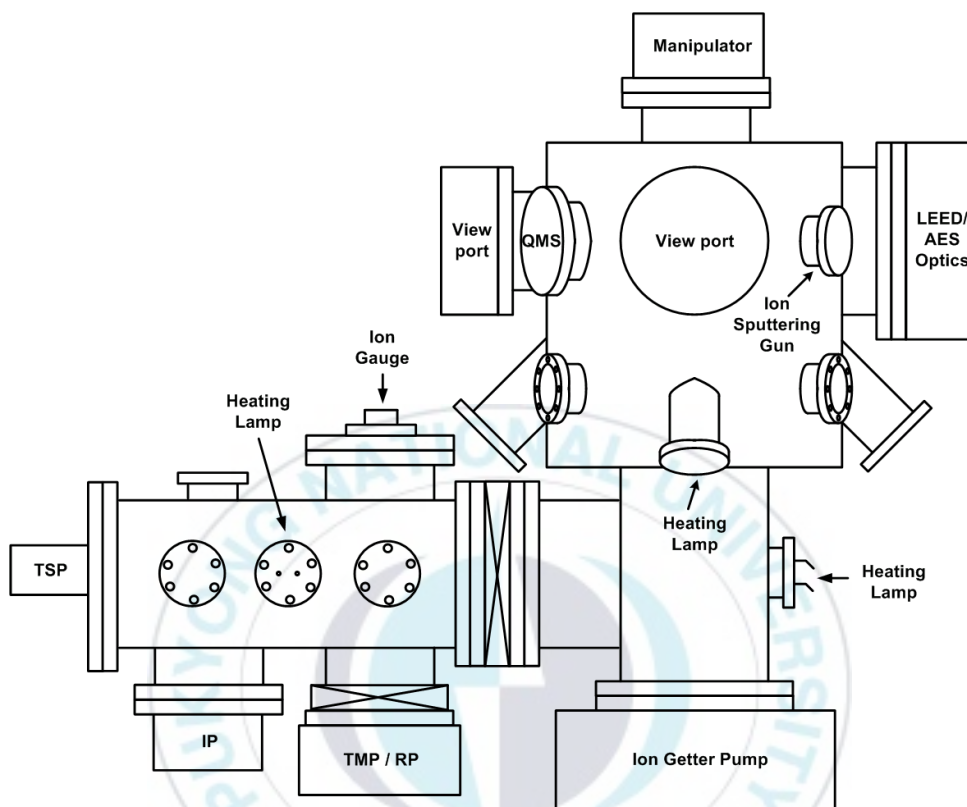


Figure 3.1 Schematic representation (front view) of the ultra-high system for LEED/AES.

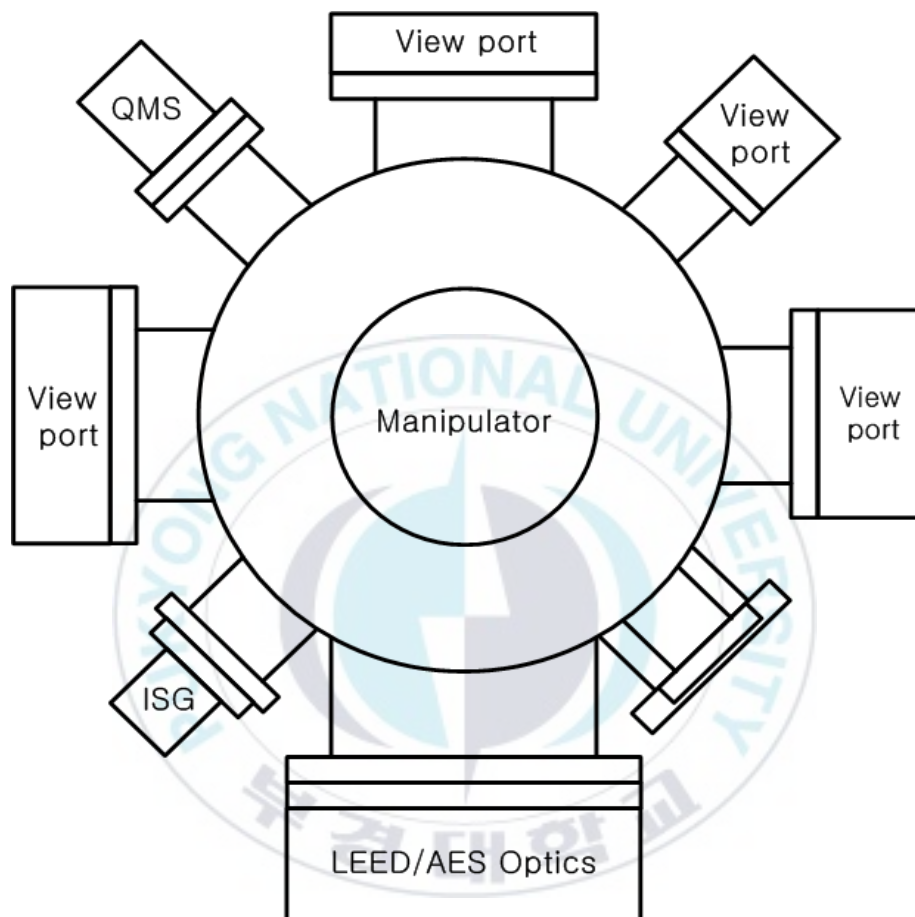


Figure 3.2 Schematic representation (top view) of the ultra-high system for LEED/AES.

3.1.2 Experimental procedure

All AES experiments were carried out in a turbomolecular-pumped ultra-high vacuum (UHV) chamber with a base pressure in the 1.0×10^{-10} torr region. The Zry-4 sample has a thickness of 1.1 mm and a surface area of 0.82 cm^2 . Its elemental composition, in wt%, is 1.31 % Sn, 0.21 % Fe, 0.11 % Cr, 0.12 % O, and the balance Zr. The Zry-4 sample was mechanically polished with abrasive paper and mechanical polisher (Buehler, gamma alumina, 0.05 micron). After polishing, the sample was sonicated for 10 min in acetone. Ammonium hydroxide (99.99% Aldrich) was stored in an equilibration flask and argon (99.99%) were connected directly to the reactive and inert section of the gas handling system, respectively. Ammonium hydroxide was purified by a few cycles of freeze-pump-thaw method and the purity of the gas was checked by a quadrupole mass spectrometer (QMS). The surface was cleaned by 3 kV argon ion sputtering below room temperature followed by annealing to 893K at a heating rate of 1.0 K/s. The cleanliness of the surface was verified using retarding field Auger electron spectroscopy (AES) with a 3 keV beam energy. When the survey scan AE of spectra were performed the energy step was 1 eV, dwell time was 100 ms, and the lock-in amplifier sensitivity was 3 mV. High resolution AE spectra were taken with 0.2 eV energy step and other factors were kept same as survey scan.

3.2 Investigation of NH₄OH on Zircaloy-4 Surfaces using X-ray Photoelectron Spectroscopy

3.2.1 Preparation of sample and operation of XPS

Surface chemical analysis ammonium hydroxide on Zircaloy 4 (Zry-4) surface was done by XPS (VG ESCALAB 2000). The energy analyzer of the XPS system was a concentric hemispherical analyzer (CHA). The base pressure in the analysis chamber was maintained lower than 1×10^{-10} torr. The X-ray source, a dual-anode source, is capable of delivering achromatic Mg K α (1253.6 eV) and Al K α (1486.6 eV) X-rays. During all experiments, spectra were obtained using Mg K α X-rays. X-ray source was at the high voltage of 15 kV, beam current of 15 mA, filament current of 4.2 A, pass energy of 50 eV, dwell time of 50 ms and energy step size of 1 eV in constant analyzer energy (CAE) mode at large area XPS (LAXPS) mode. High resolution spectra were obtained at pass energy of 20 eV, energy step size of 0.05 eV and other factors were same as LAXPS mode.

The XPS chamber was pumped by two stages of pumping system. The first one is that a turbomolecular pump (TMP) backed by a two stage rotary vane pump (RP) system pumps a fast entry air load-lock (FEAL) chamber. And the second system consists of an ion gettering pump and a Ti-sublimation pump and evacuates analysis chamber to maintain UHV condition.

The Zry-4 sample was round shape with 6.1 mm of diameter from a sheet of zircaloy-4. The composition of Zry-4 is 1.31 wt% Sn, 0.21 wt% Fe, 0.11 wt% Cr, 0.12 wt% O, balanced with zirconium. The Zry-4 sample was mechanically ground

and polished with abrasive paper and mechanical polisher (Buehler, gamma alumina, 0.05 micron). After mechanical treatment, it was ultrasonically cleaned in acetone for 10 min. Ammonium hydroxide (99.99% Aldrich) stored in an equilibration flask and argon (99.99%) are connected directly to the reactive and inert section of the gas handling system, respectively. Ammonium hydroxide is purified by a few cycles of freeze-pump-thaw method and the purity of the gas was checked by quadruple mass spectrometer (QMS) as shown in Figure 3.1. The sample current was about $1.70 \mu\text{A}$ and the argon fluence was $4.6 \times 10^{15} \text{ Ar}^+/\text{cm}^2$ per one cycle of Ar^+ sputtering (argon pressure : 3.7×10^{-8} torr). Baking of the gas line was carried out as needed to maintain the purity of the gases before introducing into the main chamber. Gas dosing was performed by backfilling the chamber through precision leak valves and gas exposures are reported in Langmuir (L) units ($1 \text{ L} = 1.0 \times 10^{-6} \text{ torr s}$). XPS experiment was performed after of ammonium hydroxide exposure.

3.2.2 Deconvolution

Our XPS data were deconvoluted using XPSPEAK software (ver 4.1) for data analysis. Obtained XPS N1s and O1s peaks were divided into two peaks but Zr3d peak was divided into several peaks according to their chemical environments. The Full Width Half Maximum (FWHM) of N1s, O1s and Zr3d peak was between 1.16~1.77, 1.53~1.88 eV and 0.99~1.89 eV, and G/L ratio of 30% (Lorentzian-30%, Gaussian-70%). The Spin-Orbit Splitting (S.O.S) of Zr 3d was 2.4 eV.

IV. Results and Discussion

4.1 Auger electron spectroscopy of Zircaloy-4

Figure 4.1 shows Zry-4 survey scan of Auger electron spectra before and after argon ion sputtering. By looking at the Auger peak-to-peak height (APPH) we indicate that C(KLL, 275 eV), N(KLL, 379 eV) and O(KLL, 512 eV) decrease after Ar^+ sputtering except Zr(MNV, 147 eV) [31]. Nevertheless oxygen peak was always detected because of the large solid solubility of O in Zr [34] and the reactive gettering nature of the surface even under UHV conditions. There are Zr Auger features below 150 eV of binding energy. We could noticed the fact that the Zr(MNV, 147 eV) feature was not clear and the surface was contaminated with carbon and oxygen in air exposed Zry-4 sample. As the argon ion sputtering cycles proceeded, the (APPH) of C(KLL) was remarkably decreased and the APPH of surface oxygen was diminished to undetectable limit and the Zr(MNV) feature was grown and getting sharper. The cleanliness of Zry-4 surface was verified with AES in terms of carbon and nitrogen contents on the Zry-4 surfaces.

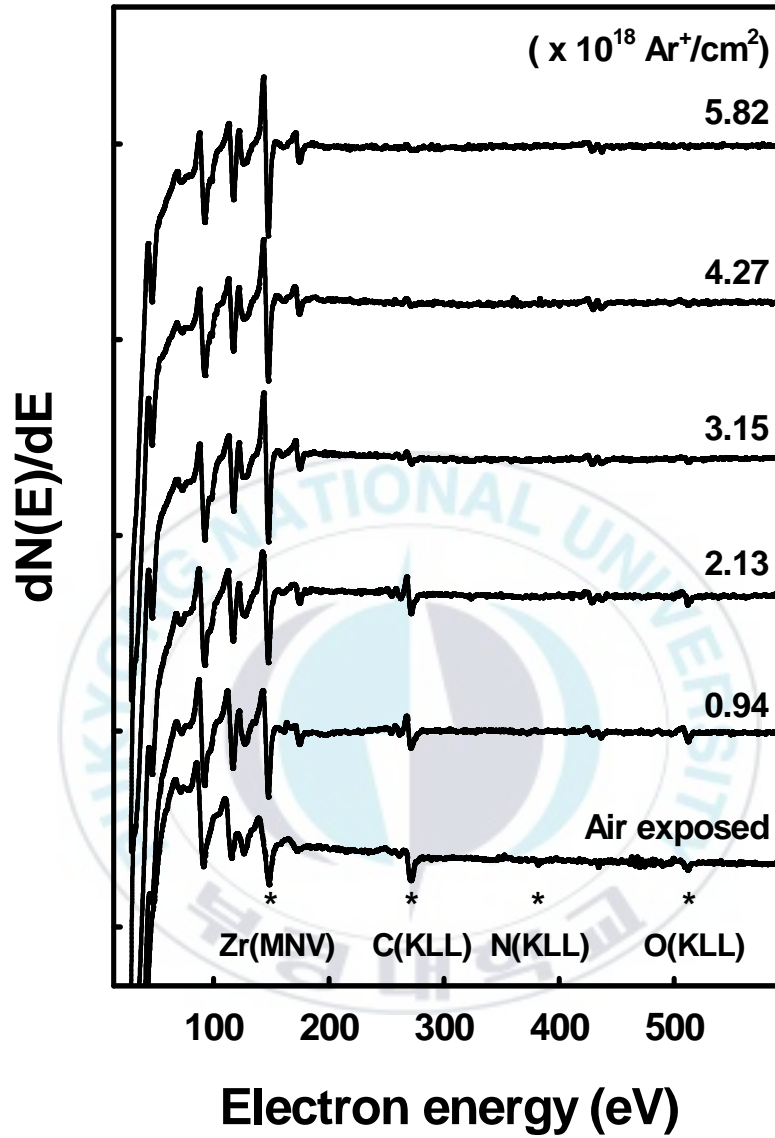


Figure 4.1 The survey AE spectra of Zry-4 before and after stepwise argon ion sputtering. The numbers at the right in the figure represent Ar fluence.

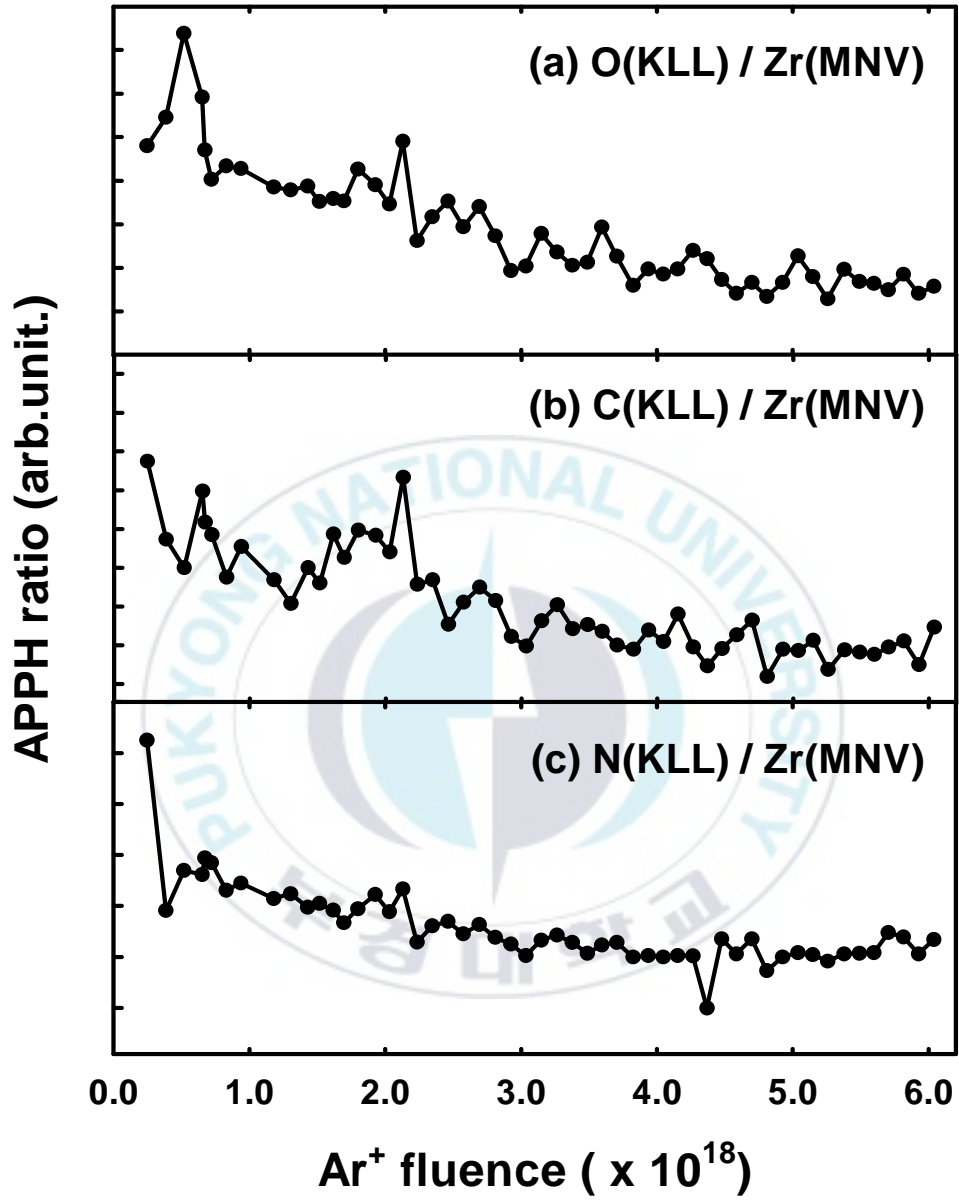


Figure 4.2 APPH ratios of Zircaloy-4 surfaces function of Ar⁺ fluence
 (a) O(KLL)/Zr(MNV), (b) C(KLL)/Zr(MNV) and (c) N(KLL)/Zr(MNV).

Figure 4.2 shows the APPH ratios of O(KLL, 512 eV) / Zr(MNV, 147 eV), C(KLL, 275 eV) / Zr(MNV, 147 eV) and N(KLL, 379 eV) / Zr(MNV, 147 eV) after stepwise argon ion sputtering to various argon fluence. As we can see in the figures, the surface of Zry-4 was reached to clean limit when the Ar fluence was about 3.5×10^{18} .

4.2 Investigation of NH₄OH on Zircaloy-4 Surfaces using X-ray Photoelectron Spectroscopy

The survey scan XPS spectra of NH₄OH/Zry-4 in the range of binding energies 0-1100.0 eV is shown in Figure 4.5. The bottom spectra represent the XPS survey scan after NH₄OH was exposed onto Zry-4 surface. The two spectra from the top are representative survey scan after stepwise Ar⁺ sputtering. The differences of NH₄OH/Zry-4 XPS features before and after Ar⁺ sputtering were focused. Prominent peaks belonging to Zr3d and O1s are clearly seen at 183.2 eV and 531.1 eV, respectively. The XPS features of C1s (286.1 eV) and N1s (397.0 eV) were changed before and after Ar⁺ sputtering.

The peak intensity of O1s decreased after Ar⁺ sputtering, however Zr3d peak intensity was nearly same before and after Ar⁺ sputtering. Carbon was also found it may be due to the amorphous carbon from carbon monoxide or carbon dioxide adsorption [32]. However, 0.32×10^{16} Ar⁺/cm² bombardment was enough to clean the Zry-4 surface in terms of carbon contamination (not shown here)

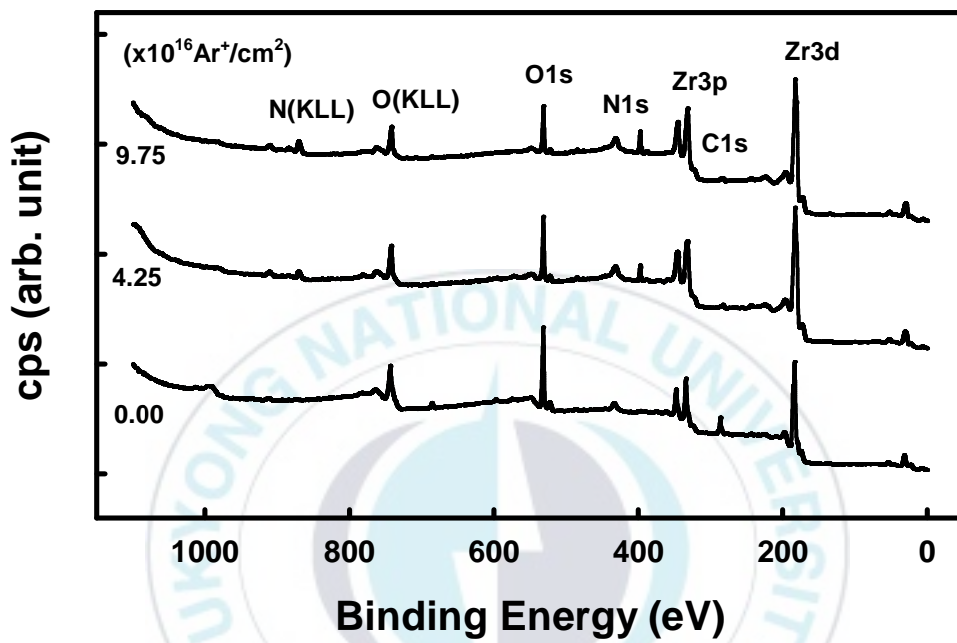


Figure 4.3 The survey XPS spectra of NH₄OH/Zry-4 before and after Ar⁺ sputtering with LAXPS mode. The numbers at the left in the figure represent Ar fluence.

Figure 4.4.1(a) presents a set of high resolution N1s XPS spectra of NH₄OH/Zry-4 following cycles of argon ion sputtering. The N1s peak intensity was remarkably growing after cycles of Ar ion sputtering. Yamamoto et al. reported that nitrogen is more stable than oxygen species on zirconium surface [21,22,33]. Weakly bound oxygen species was desorbed from the surface then nitrogen stayed under the subsurface region diffused out onto the zircaloy surface. The result was well supported previous result of Yamamoto's work. The trend of peak intensity of N1s following cycles of Ar⁺ sputtering is plotted in Figure 4.7(a). The N1s XPS spectrum was composed with a main component centered at 397.1 eV and a less intense peak centered at 398.9 eV after Ar⁺ etching, which is attributed to ammonia and zirconium nitride shown in Figure 4.4.2(b) and 4.4.2(c) [34,35]. The comparison of the data between Figure 4.4.2(b) and 4.4.2(c) reveals that, after Ar⁺ sputtering the intensities of N1s peaks from ammonia and zirconium nitride increase sharply. According to these results, we can confirm that the subsurface region nitrogen was diffused out onto the Zry-4 surface.

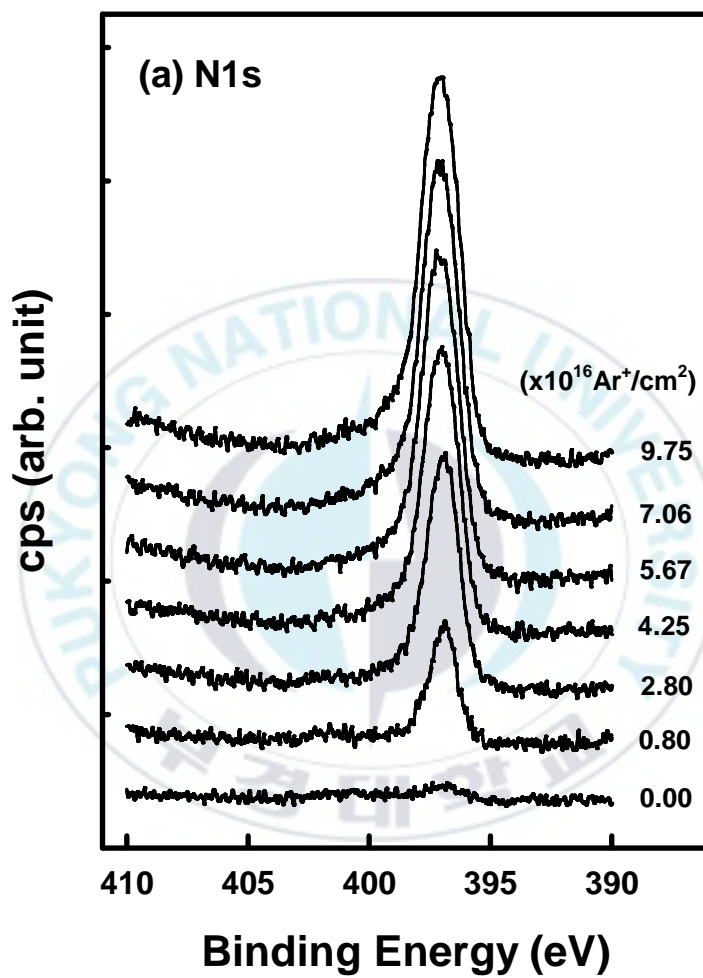


Figure 4.4.1 (a) stacked XP spectra of the N1s region after argon ion sputtering processes indicate a strong increase of N1s.

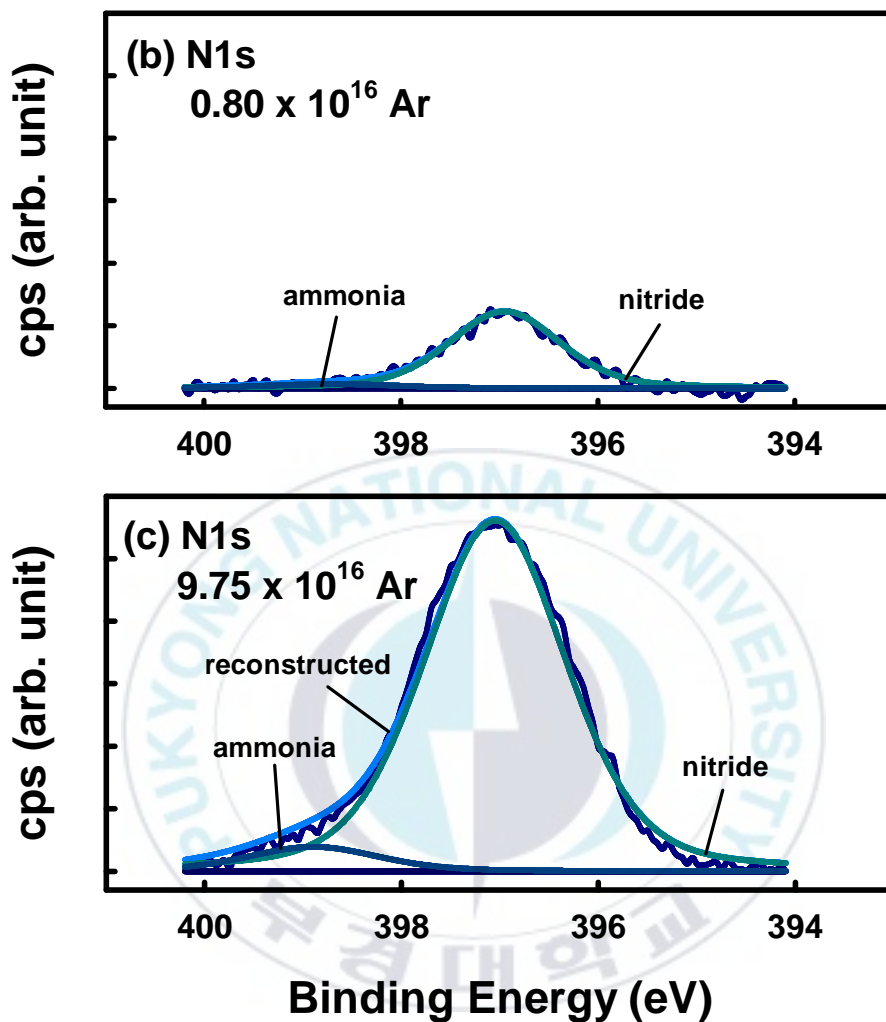


Figure 4.4.2 Deconvoluted XP spectra of the N1s region in NH₄OH/Zry-4 (b) after 0.8×10^{16} Ar⁺ sputtering and (c) after 9.75×10^{16} Ar⁺ sputtering. Wiggly lines in (b) and (c) represent raw data, smooth lines overlapped with raw data are reconstructed data and bottom solid lines are background. N1s of ammonia is centered at 387.1 eV and N1s of nitride is centered at 398.9 eV.

The representative O1s XPS spectra following cycles of Ar⁺ sputtering was stacked in Figure 4.5.1(a). The comparison of XP spectra of the O1s region before and after Ar⁺ sputtering is shown in Figure 4.5.2(b) and 4.5.2(c), respectively. The oxygen may come from surface adsorption and hydroxyl ion [32]. The deconvolution of the O1s peak in Figure 4.5.2(c) reveals two components [6,36] centered at 531.1 eV and 532.8 eV those are attributed to the hydroxyl ion and O²⁻, respectively. After stepwise Ar⁺ sputtering, total O1s peak intensity was decreased. This may happen because the surface oxygen is diffused into the bulk or sputtered out during Ar⁺ sputtering. After the concentration of oxygen near the surface region was decreased, nitrogen stayed under the surface region was diffused out to the surface region cause increasing of the N1s peak intensity. When the sample surface was clean in terms of carbon contamination by cycles of Ar⁺ sputtering, oxygen intensity of the surface is almost same shown in Figure 4.5.2(b). This phenomenon was common to zirconium system as oxygen solid solution state [37].

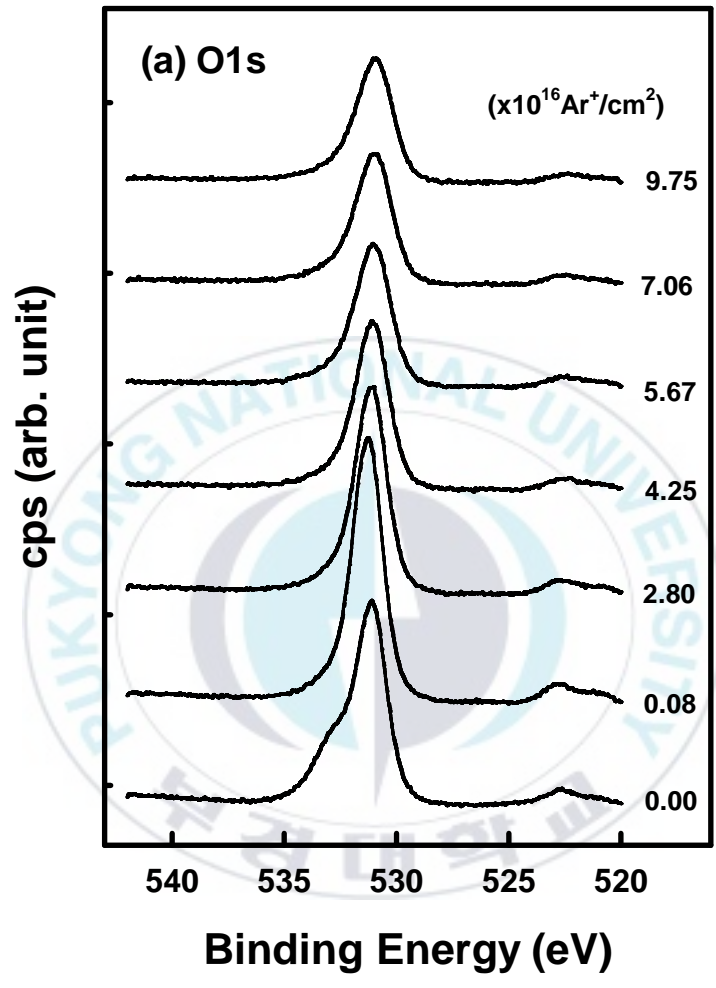


Figure 4.5.1 (a) XPS spectra of the O1s region after argon ion sputtering indicates a strong reduction of O1s.

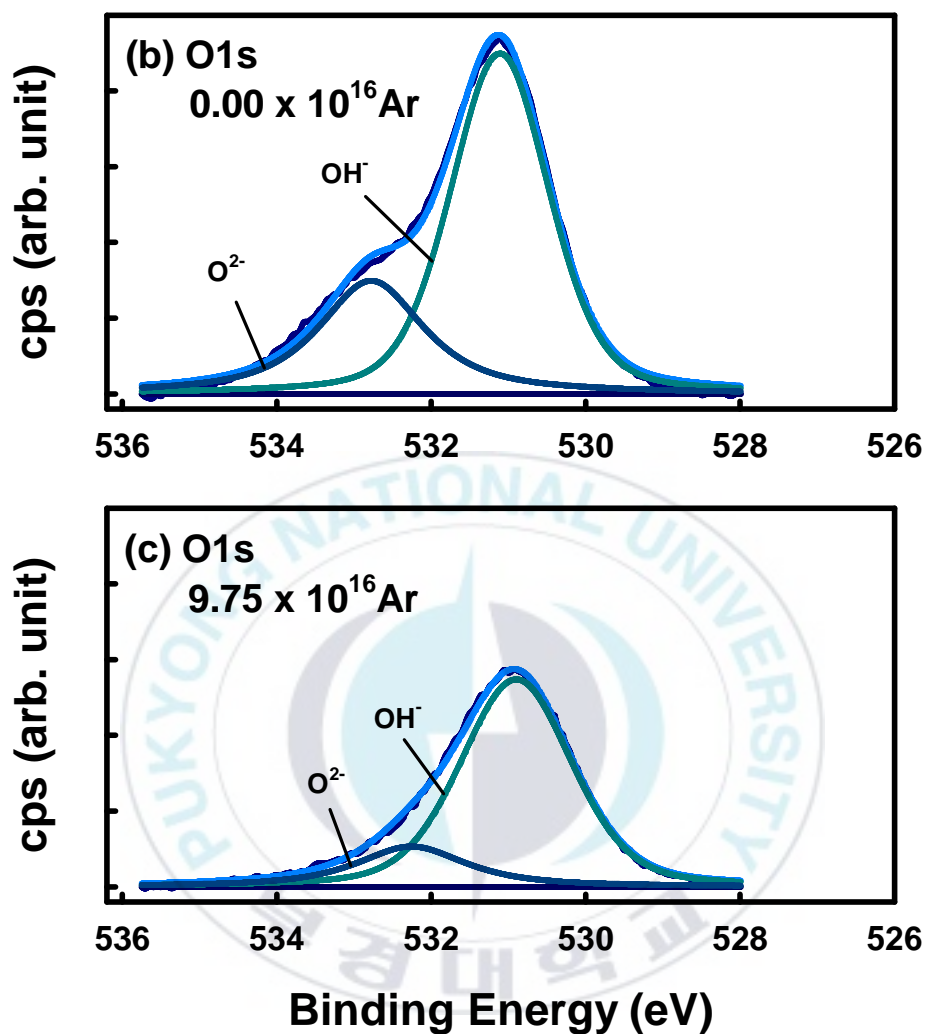


Figure 4.5.2 Deconvoluted XP spectra of the O1s region in NH₄OH/Zry-4 (b) before and (c) after Ar⁺ sputtering. Wiggly lines in (b) and (c) represent raw data, smooth lines overlapped with raw data are reconstructed data and bottom solid lines are background. The component centered at 531.0 eV is attributed to the hydroxyl ion and 532.8 eV is attributed to the presence of O²⁻ ions.

The comparison of XPS spectra of the Zr3d region before and after Ar⁺ sputtering is shown in Figure 4.6.2(b) and 4.6.2(c). Zr3d XP spectra consist of one main set of doublet i.e. the Zr3d_{3/2} and Zr3d_{5/2} peaks. After Ar⁺ sputtering, the intensities of Zr3d XP spectra did not much change but the shapes of the peaks clearly did change as we can see in Figure 4.6.1(a). Before Ar⁺ sputtering, the Zr3d XP spectra can be deconvoluted into four components, i.e. metallic Zr (179.1 eV), zirconium nitride (ZrN_x, 181.6 eV) [6], zirconium oxide (ZrO_x, 183.2 eV) and Zr⁴⁺ (Zirconia, 183.4 eV). The Zr3d peak intensity from zirconium nitride (ZrN_x) increased following Ar⁺ sputtering cycles. However, after Ar⁺ sputtering, the peak intensity of zirconium oxide (ZrO_x) decreased. This is well matched with the results of oxygen intensity was decreased and nitrogen intensity was increased by stepwise Ar⁺ sputtering.

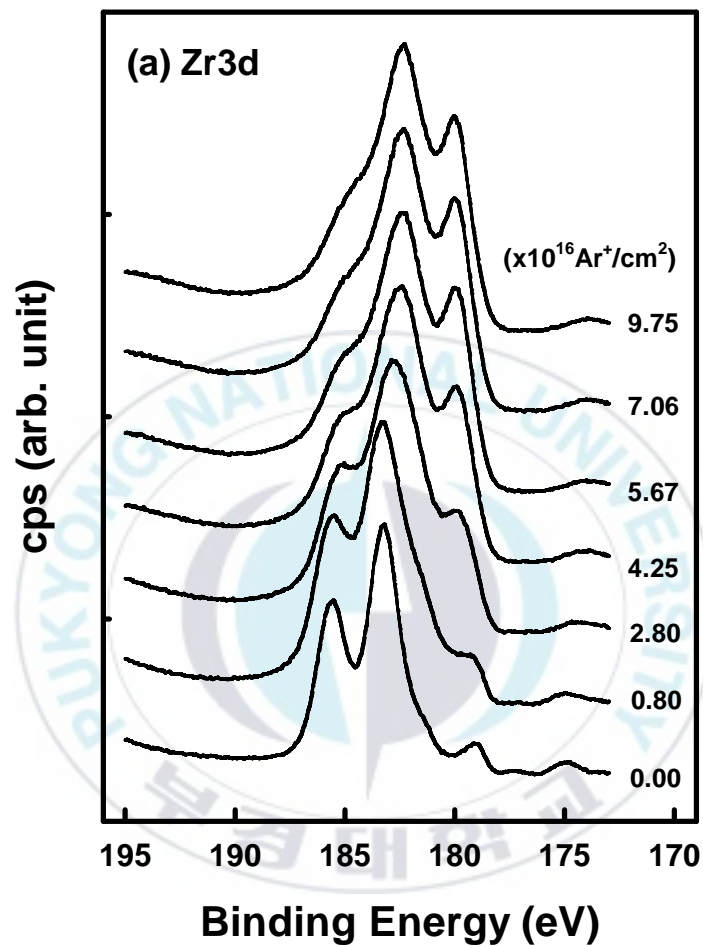


Figure 4.6.1 (a) XP spectra of the Zr3d region following cycles of Ar^+ sputtering. XPS spectra of the Zr3d region in $\text{NH}_4\text{OH}/\text{Zry-4}$ (b) before and (c) after Ar^+ sputtering.

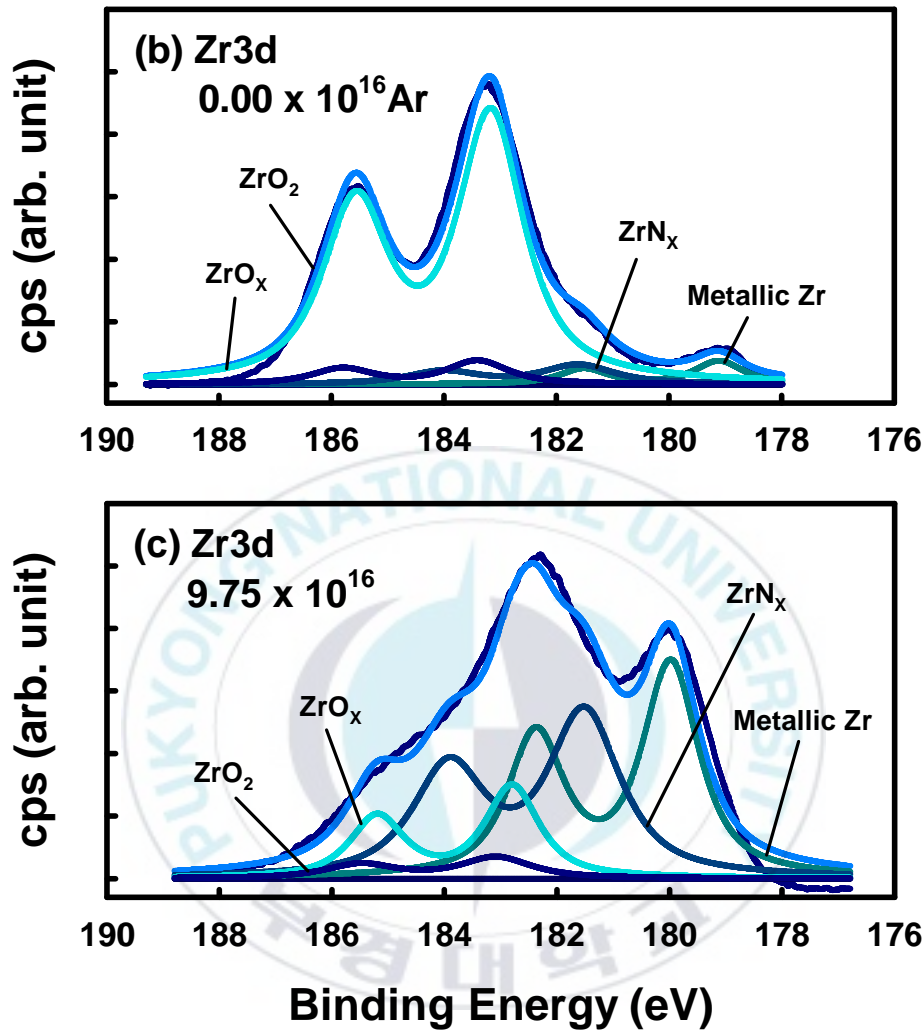
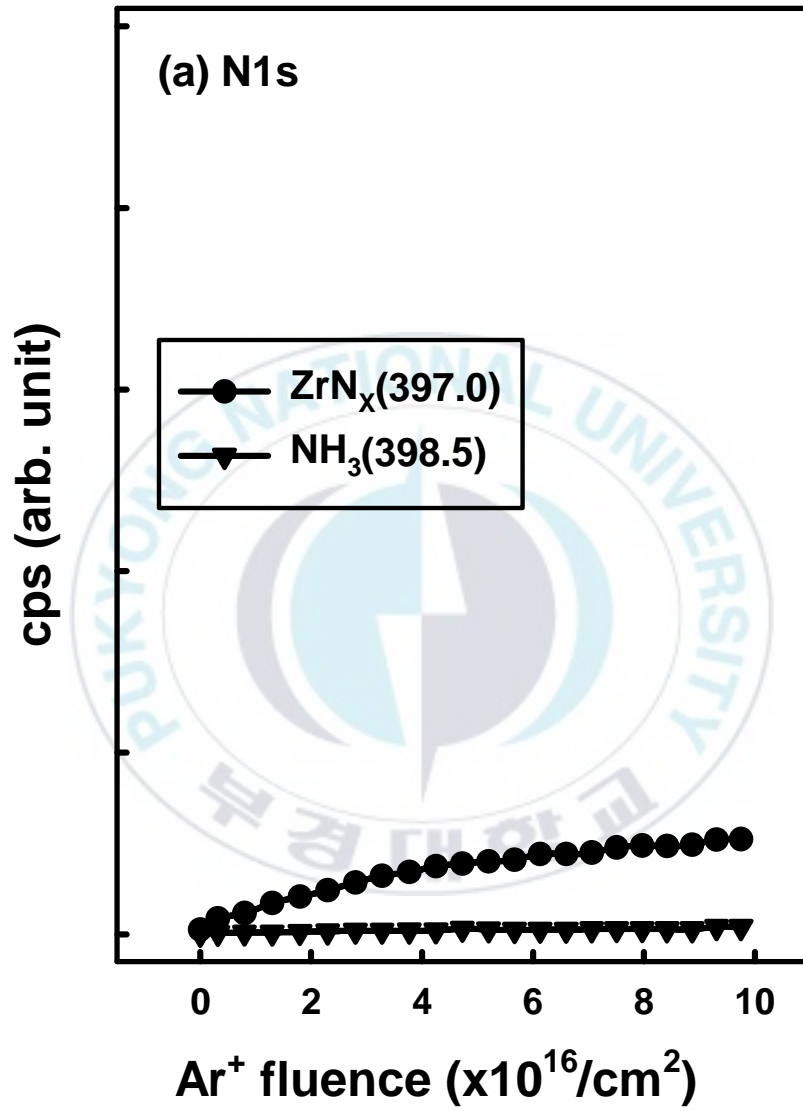
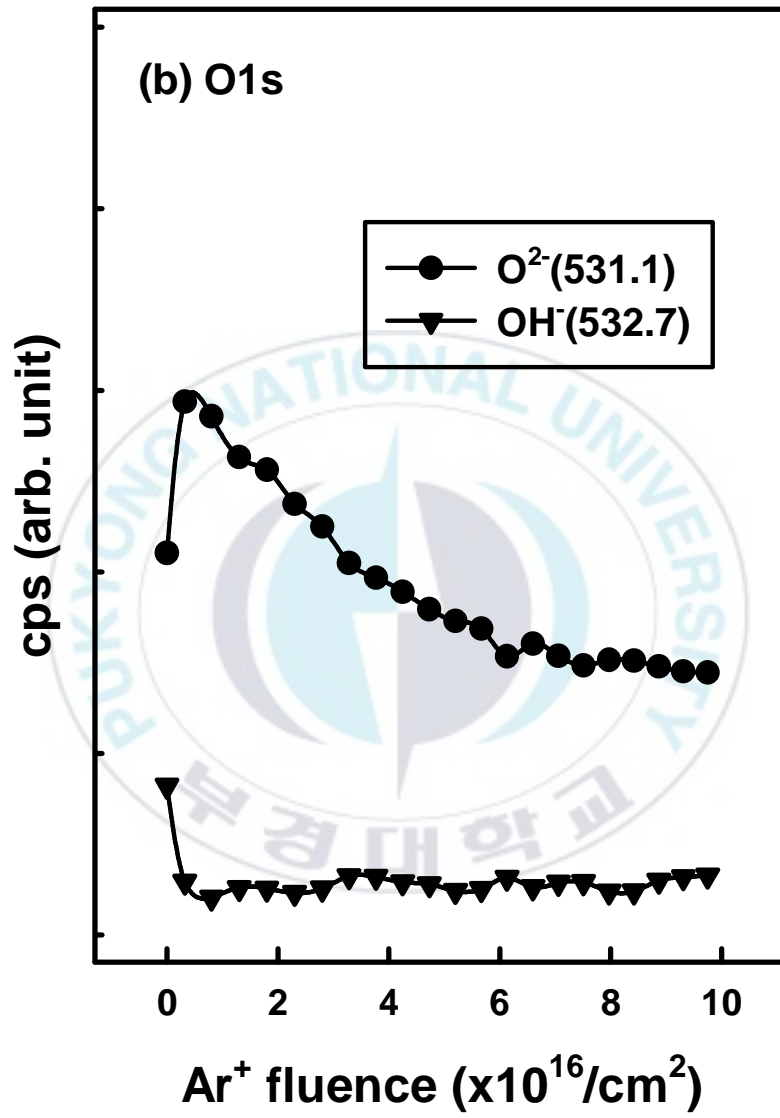


Figure 4.6.2 Wiggly lines in (b) and (c) represent raw data, smooth lines overlapped with raw data are reconstructed data and bottom solid lines are background. Zr3d of metallic zirconium is centered at 179.1 eV, Zr3d of ZrN_x is centered at 181.6 eV, Zr3d of ZrO_x is centered at 398.9 eV and Zr3d of Zr^{4+} zirconia is centered at 183.4 eV.

The Zr^{4+} intensity was nearly same before and after Ar^+ sputtering process but the peak intensity of metallic Zr increased compared to that of before the sputtering process because the surface was relatively clean. The intensity of ZrN_x was increased following cycles of argon ion sputtering because the subsurface nitrogen was diffused out onto the Zry-4. However the ZrO_x was decreased after stepwise argon sputtering according to the total O1s peak intensity was decreased shown in Figure 4.7(c).







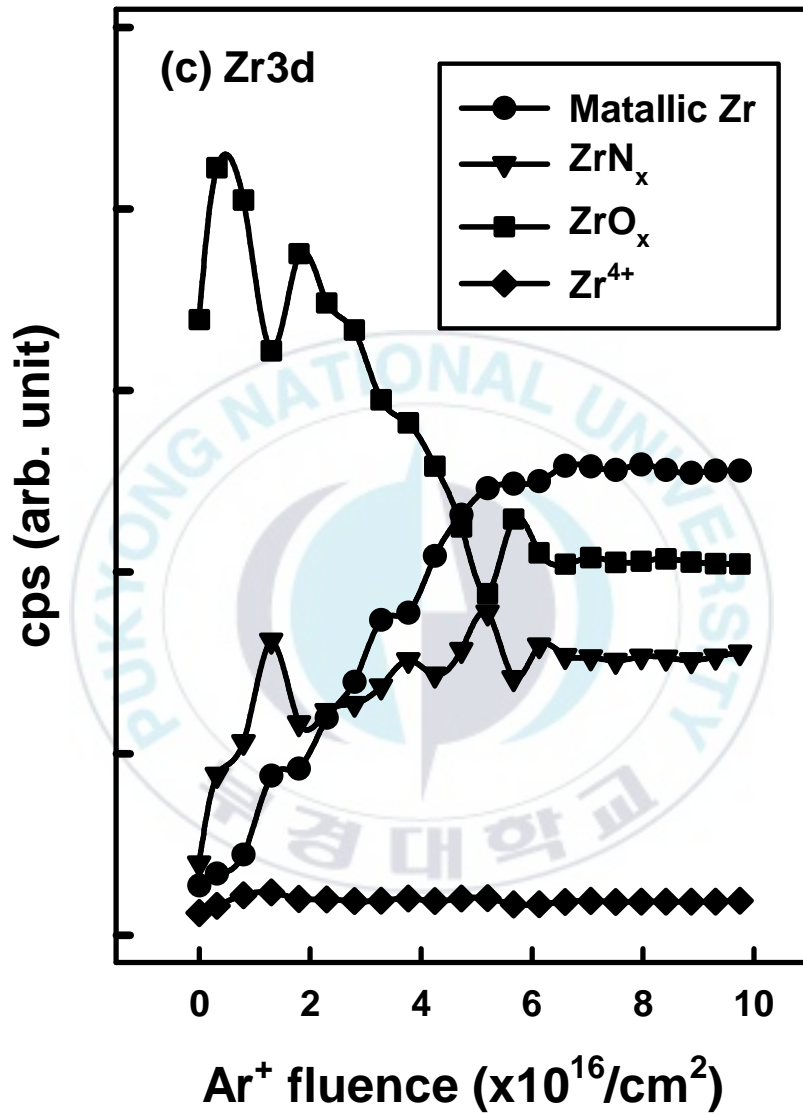


Figure 4.7 The area of deconvoluted XPS peaks of NH₄OH/Zry-4 surface as a function of argon fluence (a) N1s, (b) O1s and (c) Zr3d.

V. Conclusion

The AES experiment was performed to check the cleanliness of Zry-4 surface. The APPHs of C(KLL), N(KLL) and O(KLL) were decreased while that of Zr(MNV) was increased by following stepwise Ar⁺ sputtering. Before NH₄OH dosed on Zry-4 surface, Ar⁺ fluence of 3.5×10^{18} Ar⁺/cm² was enough to clean the Zry-4 surface in terms of carbon contamination. The interaction of NH₄OH with Zry-4 surface was investigated using XPS methods after cleanliness Zry-4 was verified. The interaction of NH₄OH with Zry-4 was investigated using XPS methods. The results show that the changes of XPS intensities, which are O1s, N1s and Zr3d, by stepwise Ar⁺ sputtering. During the stepwise Ar⁺ sputtering, oxygen peak intensity was decreased while nitrogen peak intensity was increased. This happened because the weakly bound oxygen was diffused into the bulk or desorbed out from the surface then the nitrogen stayed subsurface region diffused out to the deficient sites on the surface region. This oxygen and nitrogen intensity conversion caused increasing of zirconium nitride intensity and decreasing of zirconium oxide intensity. After the Ar fluence of 6.0×10^{16} Ar⁺/cm² was applied to the NH₄OH/Zry-4 system, the peak intensities of O1s, N1s and Zr3d were stayed same.

VI. Reference

- [1] Ahmad, M. Akhter, J. I. Ali, G. Akhtar, M. Choudhry, M. A. *J. Alloys Comp.* **2006**, 426, 176.
- [2] Meyer, G. Kobrinsky, M. Abriata, J. P. Bolcich, J.C. *J. Nucl. Mater.* **1996**, 229, 48.
- [3] Hsu, H.-H. *J. Alloys Comp.* **2006**, 426, 256.
- [4] Lim, B. H.; Hong, H. S.; Lee, K. S. *J. Alloys Comp.* **2003**, 312, 134.
- [5] Wiame, H.; Centeno, M.-A.; Picard, S.; Bastians, P.; Grange, P. *J. Eur. Ceram. Soc.* **1998**, 18, 1293.
- [6] Peng, D. Q. Bai, X. D. Pan, F. Sun, H. Chen, B. S. *Appl. Surf. Sci.* **2005**, 252, 1793.
- [7] Inoue, M. Yamashita, M. Suganuma, K. Nunogaki, M. *J. Nucl. Sci. Technol.* **2001**, 38, 980.
- [8] Chemelle, P. Knorr, D. B. Van Der Sande, J. B. Pelloux, R. M. *J. Nucl. Mater.* **1983**, 113, 58.
- [9] D.R. Lide (Ed.), "CRC Handbook of Chemistry and Physics 75th Edition", CRC Press, USA, 1994 (Section 11 and 12).
- [10] Fromm, E. Jehn, H. *Bull. Alloy Phase Diagrams* : **1984**, 5(3), 323.
- [11] Konev, V. N. Nadolskii, A. L. Minyacheva, L. A. *Oxidation Metals* : **1997**, 47(3/4), 237.
- [12] Yamanaka, S. Miyake, M. Katsura, M. *J. Nucl. Mater.* **1997**, 247, 315.
- [13] Galan, P. P. Sanz, L. Rueda, J. M. *Surf. Interf. Anal.* **1990**, 16(1-12), 535.
- [14] Choo, K. N. Kim, Y. S. *J. Nucl. Mater.* **2001**, 297, 52.
- [15] Zhang, C.-S. Norton, P. R. *J. Nucl. Mater.* **2002**, 300, 7.
- [16] Roustila, A. Chêne, J. Séverac, C. *J. Alloys Comp.* **2003**, 356, 330.

- [17] Cox, B. J. *Alloys Comp.* **1997**, 256, 244.
- [18] Khatamian, D. J. *Alloys Comp.* **1997**, 253, 471.
- [19] Bellanger, G. Rameau, J. J. *J. Mater. Sci.* , **2000**, 35, 1759.
- [20] Yau, T. L. Paul, B. O. Henson, R. H. *Chem. Process*, **1999**, 62, 70.
- [21] Kang, Y. C. Ramsier, R. D. *Vacuum*, **2002**, 64, 113.
- [22] Stojilovic, N. Kang, Y. C.; Ramsier, R. D. *Surf. Interface Anal.* **2002**, 33, 945.
- [23] Hong, H. S.; Kim, S. J.; Lee, K. S. *J. Nucl. Mater.* **1999**, 273, 177.
- [24] Stojilovic, N. Ramsier, R. D. *Appl. Surf. Sci.* **2006**, 252, 5839.
- [25] Stojilovic, N. Bender, E. T. Ramsier, R. D. *J. Nucl. Mater.* **2006**, 348, 79.
- [26] Chohen, P. Water coolant technology of power reactors. La Grange Park: Am. Nuc. Sc. **1980**.
- [27] Stojilovic, N.; Bender, E.T.; Ramsier, R.D. *Appl. Surf. Sci.* **2005**, 252, 1806.
- [28] Chrysostomou, D.; Flowers, J.; Zaera, F. *Surf. Sci.* **1999**, 439, 34.
- [29] C. L. Hedberg (Ed.), "Handbook of Auger Electron Spectroscopy 3rd Edition", Physical Electronics, Inc., 1995.
- [30] G. Attard, C. Barnes (Ed.), "Surface", OCP press, USA, 1998 (Section 2).
- [31] Kang, Y. C. Ramsier, R. D. *J. Nucl. Mater.* **2002**, 125, 303.
- [32] Gu, Y.; Guo, F.; Qian, Y.; Zheng, H.; Yang, Z. *Mater. Lett.* **2003**, 57, 1679.
- [33] Yamamoto, M.; Kurahashi, M.; Chan, C. T.; Ho, K. M.; Naito, S. *Surf. Sci.* **1997**, 387, 300.
- [34] Rizzo, A. Signore, M. A. Mirengi, L. Serra, E. *Thin Solid Films* **2006**, 515, 1313.
- [35] Benia, H. M. Guemmaz, M. Schmerber, G. Mosser, A. Parlebas, J. C. *Appl. Surf. Sci.* **2003**, 211, 146.
- [36] Zhu, X. L. Liu, S. B. Man, B. Y. Xie, C. Q. Chen, D. P. Wang, D. Q. Ye, T.C. Liu, M. *Appl. Surf. Sci.* **2007**, 253, 3122.
- [37] Tanabe, T.; Tomita, M. *Surf. Sci.* **1989**, 222, 84.

VII. Appendices

1. Appendix A : Procedure for Argon ion sputtering

1. Check the pressure of main chamber.
2. Ion pump off (start → high voltage off → power off).
3. Unplug all electric lines (power lines for sample heating / thermocouple).
4. Set the manipulator for Ar sputtering.
5. Install magnet and watching the position of arrow using manipulator.
(μA scale).
6. Open MGV 2 turns from closed position.
7. Ground the sample.
8. Main switch on (ion gun controller ISES).
9. Turn on "Beam Energy" to 5 kV (turn right ☉).
10. Open Ar leak valve.

Measure sample current every 5 min for 15 min

11. Close Ar leak valve.
12. Turn down "Beam Energy" to zero (turn left ☺).
13. Main switch off.
14. Open main gate valve slowly watching the pressure gauge.
15. Ion pump on (power → high voltage on → start).

16. Anneal the sample.

target T. - Zry-4 : 620 °C / Pt₃Co : 430 °C

After annealing

17. Temperature controller power off.

18. Unplug thermocouple and heater power line.

19. Ground the sample using multimeter (μ A).

Sputtering position

Zry-4 x : 15.1

y : 18.5

z : 70.8

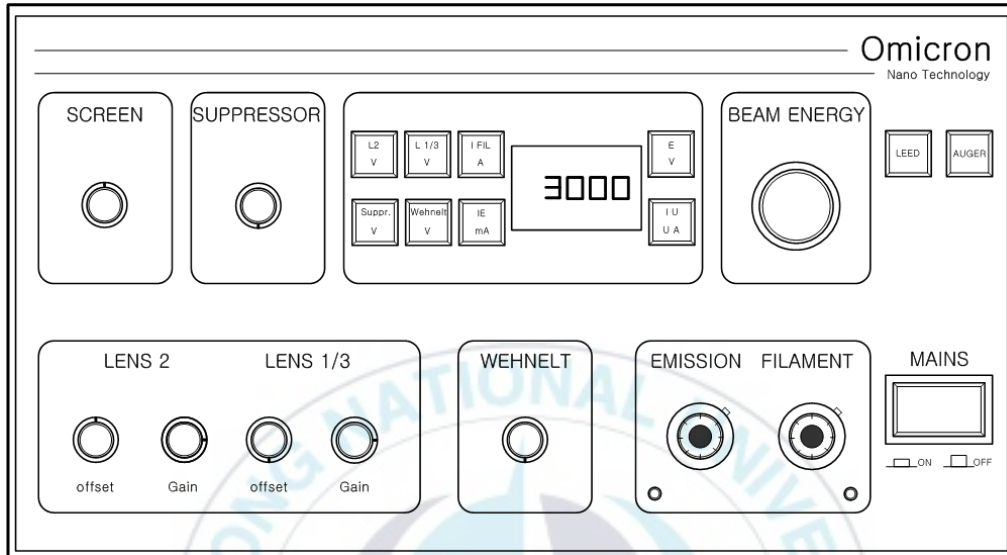
θ : 22.8

P(Ar)=1.0 x 10⁻⁶ torr

Sample current \approx 18 μ A

Free state for rotation - x : 15.1 / y : 18.5

2. Appendix B : Procedure for Auger electron spectroscopy (AES) experiments



1. Warm up the electronics for 30 min.
2. Make sure the sample has been sputtered, annealed and cooled.
3. Set the sample manipulator for AES experiments.

Zry-4 x : 8.21

y : 10.615

z : 68.74

θ : 179.5

4. Set the LEED/AES optics for AES experiments by pushing "Auger" button.
5. Ground the sample by multimeter (μA range).
6. Turn ("FILAMENT CURRENT" "SCREEN") knobs to fully anticlockwise.
7. Turn "EMISSION" knob to fully clockwise.

8. Turn on MAIN POWER ⇒ Push Auger button.
9. Increase Filament current up to "1.17" A.
10. Set beam energy to 3000 eV.
11. Software
 - ① DATA Auger click.
 - ② SET UP ⇒ Experiment properties.
 - ③ Chose the element ⇒ O.K.
 - ④ Right mouse button ⇒ Data processing ⇒ Differentiate Spectra.
 - ⑤ RUN click.



3. Appendix C : Eurotherm PID setting

<Eurotherm 2404 setting>

1) From room temperature

- Pb : 900
- ti : 17
- td : off → res : 0.0
- hcb : auto → res : 0.0
- Lcb : auto

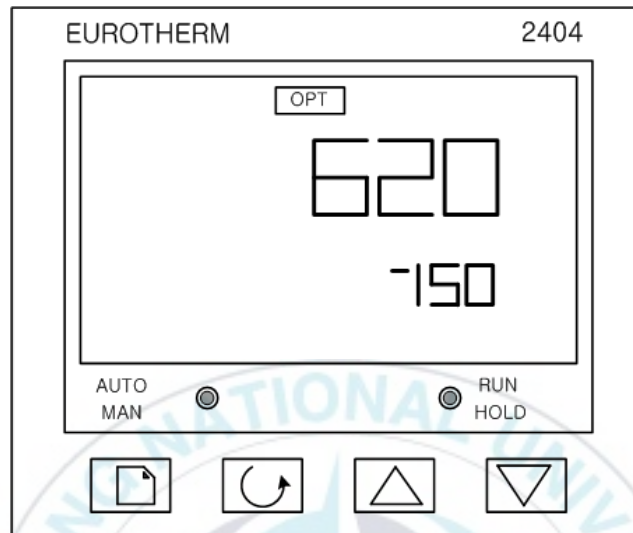
2) From low temperature @ ~ -60 ℃

- Pb 1 : 588
- ti 1 : 40
- td 1 : off
- hcb 1 : auto
- Lcb 1 : auto

- Pb 2 : 900
- ti 2 : 30
- td 2 : off
- hcb 2 : auto
- Lcb 2 : auto

※ When the speed of output power is slow → OPrr → "OFF"

4. Appendix D : TPD experiment



1. Push the "RUN/HOLD" button and wait about for 6 min.
→ During that time the HOLD letter is going to flickering.
2. When the DC Volt Meter changed press the "RUN/HOLD".
3. Press  button 3 times (Program list sign will show up).
4. Press  button twice and than  button twice (band "off" will appear).
5. After "RUN/HOLD" button flickering, press the "RUN/HOLD" button.
5. Annealing is going to "START".

Korean Abstract

전자 분광학을 이용한 지르칼로이-4와 수산화 암모늄의 상호작용

Hye Yoon Jung

Graduate School of Education

Pukyong National University

Abstract

X선 광전자 분광학으로 지르칼로이-4와 수산화 암모늄의 상호작용을 연구하였고 오제 전자 분광학으로 표면의 깨끗한 정도를 확인하였다. 지르칼로이-4와 수산화 암모늄의 표면화학을 연구하기 위해 질소 1s, 산소 1s 그리고 지르코늄 3d 궤도의 광전자 결합에너지가 조사되었다. 질소 1s 피크크기는 실온에서 지르칼로이-4에 수산화 암모늄을 투여시킨 후 아르곤 이온 스퍼터링이 계속 진행 될수록 급속히 증가하였다. 그 이유는 표면안에 있던 벌크한 질소가 지르칼로이-4 표면으로 흘러 나왔기 때문이다. 그러나 표면에 있던 산소는 아르곤이온 스퍼터링이 진행됨에 따라 산소 1s 피크크기가 감소되었는데 이는 벌크안으로 산소가 들어갔거나 아르곤 이온 영향 때문에 탈착되었다. 수십번의 아르곤이온 스퍼터링 후 지르코늄 3d의 피크크기는 변화하지 않았으나 피트들의 형태가 바뀐 것을 관찰할 수 있었다. 이는 아르곤 이온 스퍼터링 하는 동안 지르코늄의 산화상태가 변했기 때문인 것을 알 수 있었다. ZrN_x 의 지르코늄 3d 피크크기는 질소 1s의 크기가 증가함으로써 증가했으나 하이드록시 이온의 감소 때문에 ZrO_x 의 지르코늄 3d 피크크기는 감소하였다. 아르곤 이온 스퍼터링 과정 후 깨끗한 지르코늄의 크기는 거의 같음을 관찰하였으나 금속 지르코늄의 피크 크기는 스퍼터링 과정 전과 비교 하였을 때 증가함을 관찰되었는데 이는 표면이 깨끗해졌기 때문이다.

Acknowledgement

I would like to express my sincere gratitude to Prof. Yong-Cheol Kang for his continuous guidance, encouragement and advise in this study. I would also like to thank my referees Prof. Ju Chang Kim and Prof. Don Kim for all their warm help and valuable comments concerning this work. My thanks also go to my teachers in the Department of chemistry at the Kyung Sung University. They all have guided and encouraged me.

I also thanks all graduate students, Young Hwa Kim, Ji Hye Kwon, Im Sung Shin, Han Young Park, Eun Ju Cho, Hyoun Jung Seok and Gyung Sun Oh, for sharing lots of precious memories for two and half years. I also thanks all my friends, Kim Bi, Cho Eun Young, Cho Su Mi, Kim Min Ji, Park Kyung Moon, Kim Hyo Jin, Hong Yeon Jung, Jang Yoon Jung, Lee Yu Jin, Choi Kyung Hye, Kim Sung Kyun, Park In Woo, Jung Yo Han, Sung Hea Moon, Im Jung Hwan, Jun Tae Hong, Lee Jae Hyung, Lee Dong Gyu and Kim Ji Hun for their love and support. My thankful acknowledgements are given to colleagues; Ju-Yun Park, Se Won Jung and Mi Sun Chun for their affections in the surface analysis laboratory.

My unmeasurable appreciations are expressed to my family members for their endless assistances.